ENGINEERING COMPUTATIONS, VOL. 8, 195–213 (1991)

CONTRIBUTED Papers

THREE-DIMENSIONAL TRANSIENT ANALYSIS OF A SINGLE SUBMERGED CYLINDRICAL SHELL

R. K. SINGH

Reactor Engineering Division, Bhabha Atomic Research Centre, Trombay, Bombay 400 085, India

T. KANT

Department of Civil Engineering, Indian Institute of Technology, Powai, Bombay 400 076, India

AND

A. KAKODKAR

Reactor Engineering Division, Bhabha Atomic Research Centre, Trombay, Bombay 400 085, India

ABSTRACT

Three-dimensional transient analysis of a submerged cylindrical shell is presented. Three-dimensional trilinear eight-noded isoparametric fluid element with pressure variable as unknown is coupled to a nine-noded degenerate shell element. Staggered solution scheme is shown to be very effective for this problem. This allows significant flexibility in selecting an explicit or implicit integrator to obtain the solution in an economical way. Three-dimensional transient analysis of the coupled shell fluid problem demonstrates that inclusion of bending mode is very important for submerged tube design—a factor which has not received attention, since most of the reported results are based on simplified two-dimensional plane strain analysis.

KEY WORDS Submerged shells Transient analysis Fluid–structure interaction Finite elements

INTRODUCTION

Transient analysis of submerged structures and components is an important problem which has been the focus of research activity[1–12] in the last two decades. The dynamic behaviour of structures is well understood if the surrounding fluid is known to have negligible coupling effect. However, the dynamic behaviour of the submerged structure is significantly affected if the displaced fluid mass is significant compared with the structure mass. Simplified added mass analysis of coupled fluid–structure interaction problem has been attempted[13–16]. However, this approach is suitable only for those cases where fluid oscillation frequencies are well separated from the structure predominant frequencies. The mechanism of fluid–structure interaction problem is described by the oscillations induced in the fluid either due to structural motion or due to some accident condition which may induce pressure pulse in the acoustic medium. The

0264–4401/91/030195–19$2.00 *Received April 1990*

pressure field is influenced by the structural motion, as well as the structural motion is also influenced by the pressure field of the surrounding fluid. Thus this transient phenomenon has to be studied in a coupled manner. This becomes more important if coupled modes are excited where the added mass approach or a two step decoupled analysis may become even unconservative[1–4]. In the latter case the fluid response is first obtained, assuming the structure to be rigid and the resulting pressure field is then imposed on the structure in the second step to obtain the structural response.

Earlier studies on the fluid–structure interaction problems were made by Bathe and Hahn[1], Liu and Chang[2], Liu[3], Belytschko[4], Akkas *et al.*[5], Wilson and Khalvati[6], Shantaram *et al.*[7] and Deshpande *et al.*[8]. The basic methodology applied in these studies is known as pseudo elastic approach. In this method the shear modulus is set to zero in the fluid domain and the fluid–structure interface is constrained to have normal displacement continuity. The eigen value analysis indicates the presence of zero energy modes as described by Akkas *et al.*[5]. Wilson and Khalvati[6] have suggested a method to select an optimum penalty parameter so that these spurious modes can be suppressed. In this approach irrotational flow condition is enforced. Deshpande *et al.*[8] have also come out with an optimum penalty parameter to couple the structure and fluid meshes which is a function of the density of fluid along with the acoustic speed in the fluid medium. Au-Yang[9] defines this method as continuum mechanics or structure mechanics approach. This pseudo elastic approach is suitable for a limited class of problems, such as linear behaviour of fluid. Moreover it does not turn out to be economical for a three-dimensional (3D) transient analysis even in the case of a linear problem due to large size of the fluid domain the number of discrete equations become very large.

Another approach which is very promising is the method of partitioning as suggested by Park and Felippa[17], Felippa and Geers[18]. In this approach the various interacting fields are staggered and then the field variables which are required by the neighbouring coupled fields, are transferred mutually in a sequential manner. Historically this second approach is older than the pseudo elastic approach the details of which can be seen in the work of Zienkiewicz *et al.*[19,20]. They had described a finite element formulation with pressure variable for the fluid domain and displacement variable for the structural domain. However, this did not gain popularity until recently. The major limitation of this approach is that the system of equations become unsymmetric and the band width becomes very large due to the coupling terms. Paul[10] has explored this technique for two-dimensional fluid–structure interaction problems using a staggered approach. The present authors have developed a two-dimensional fluid–structure interaction code FLUSOL[11] for plane stress, plane strain and axisymmetric problems with continuum elements along with a three-dimensional fluid–shell interaction code FLUSHEL[12] using a method of partitioning. The band width problem is overcome by assigning a separate equation numering system for coupling terms which are active only at the fluid–shell interface. Three-dimensional transient analysis is carried out by integrating fluid and shell meshes at each time step by transferring fluid pressure on the shell surface and shell normal acceleration to the fluid domain in an iterative manner. The advantage of this method is that the number of field variables can be optimized significantly. For example, in code FLUSHEL the fluid behaviour is obtained by trilinear fluid elements with only pressure variable as unknown at each node point. The structure response is obtained by nine-noded Lagrangian C^0 continuous degenerate shell element. The basic shell element of Ahmad *et al.*[21] has undergone significant improvement over the last two decades. Studies with regard to locking behaviour and zero energy modes have helped to improve the performance of this element. The details of this can be seen in the works of Hughes[22], Belytschko[23] and Hinton and Owen[24]. Performance comparison by Pugh *et al.*[25] has shown that out of four, eight, nine, twelve and sixteen noded quadrilateral elements,

nine-noded Lagrangian degenerate shell element gives optimum combination of accuracy and economy. Belytschko[23] and Milford and Schnobrich[26] have recently developed efficient two-dimensional degenerate shell element based on explicit through thickness integration. In code FLUSHEL we have used this shell element which results in considerable economy in terms of CPU time and storage space particularly on small computers for three-dimensional transient problems. The second advantage of the method of partitioning is that it is very suitable for modular adoptation. Any fluid transient code, either based on finite difference, finite element or boundary element can be coupled to this and the fluid–structure interaction effect can be studied. This gives tremendous versatility for expansion of the code and transient analysis of unexplored areas of non-linear fluid and non-linear structure can be carried out which are very important for nuclear reactor and spacecraft safety analysis. Modular adaptation of the code will also be very suitable for large size multifield coupled problems in parallel processing environment[27].

Another important aspect of transient analysis is the selection of optimum integrator for integrating ordinary differential equations (which are of second order for the present case) resulting from semi-discretization. There are two well known methods available: implicit method and explicit method[22,28–33]. Implicit methods are unconditionally stable and larger time steps are permitted depending on the order of accuracy required. This depends on the number of significant modes which are to be included by the integrator in the numerical integration process. This methods requires large CPU time and storage space as the resulting simultaneous equations by temporal discretization have to be solved at each time step. On the other hand, the explicit methods are conditionally stable and time step size depends on the minimum time period of the mesh. The minimum period of the mesh is bounded by the minimum period of an individual element[34]. The advantages of the explicit method are that the CPU time required for each time step is very small and the storage space is also very small, since factorization and back substitution of coefficient matrix is not required in this case. In case of fluid–structure interaction problems the wave speeds in the two domains are of varying order, thus a practical and economical analysis is possible by taking advantage of both the explicit and implicit methods. Explicit scheme for the fluid domain and implicit scheme for the structure domain give optimum combination of computational effort, storage space and CPU time as demonstrated in this paper.

We describe the theory of the coupled shell fluid dynamics problem used in the code FLUSHEL where shell dynamics and fluid transient problem are formulated by finite element method. We then describe the coupled field equation solution scheme. Transient analysis of a submerged cylindrical shell is then presented. First two-dimensional analysis is presented and compared with the reported results. Further three-dimensional transient analysis is given where the shell is assumed to be simply supported and clamped at ends. The analysis shows the importance of bending mode and three-dimensional fluid field for such coupled three-dimensional transient problems.

COUPLED SHELL FLUID INTERACTION PROBLEM

Coupled shell–fluid interaction problems can be amicably analysed by the method of partitioning as demonstrated by Singh *et al.*[12]. In this approach semidiscrete coupled second order ordinary differential equations of shell dynamics and three-dimensional fluid transient are integrated by Newmark's method. The shell normal accelerations are transferred to the fluid domain and fluid pressures are applied at the shell surface at each time step on the interaction boundary in an iterative manner. The transfer of interface data from one field to another field at the interaction boundary is carried out in an economical way by keeping only interface nodes of both the fields

as active degrees of freedom in skyline storage scheme. This approach results into optimum storage requirement for coupling matrices as described in this section.

Three-dimensional fluid transient analysis

The fluid transient behaviour can be efficiently obtained by using pressure formulation for the fluid domain. This approach has certain advantages for three-dimensional problems. Here the number of variables for the fluid domain are the minimum compared to the displacement formulation. The pressure field obtained from this analysis can be directly used for shell dynamics problems. The fluid field is discretized by trilinear eight noded brick elements. This results into significant economy since in the majority of the cases the fluid domain is of a large extent and the number of equations have to be limited to an extent so that the fluid loading on the shell surface is adequately defined. The shell response should be more accurately defined hence a higher order element may be used for discretization of shell domain.

The governing acoustic wave equation for an inviscid compressible fluid with small displacement assumption is given in terms of dynamic pressure p and acoustic speed c as

$$\nabla^2 p = \frac{1}{c^2}\ddot{p} \text{ in fluid domain } \Omega_f \tag{1}$$

The pressure gradients at the fluid boundary Γ_f is defined as:

$$p,n = -\varrho_f \ddot{u}_n \text{ at the interaction boundary } \Gamma_I \tag{2}$$

$$p,n = -\ddot{p}/g \text{ at the free boundary } \Gamma_F \tag{3}$$

$$p,n = -\dot{p}/c \text{ at the radiating boundary } \Gamma_R \tag{4}$$

Here ϱ_f, $\ddot{u}_n$ and g are the fluid density, shell normal acceleration and acceleration due to gravity, respectively. The boundary condition for the prescribed pressure field is given as:

$$p = p^s \quad \text{on} \quad \Gamma_p \tag{5}$$

Thus the fluid boundary Γ_f is completely defined by augmenting the above definitions.

$$\Gamma_f = \Gamma_I + \Gamma_R + \Gamma_F + \Gamma_p \tag{6}$$

Equation (1) along with the boundary conditions (2)–(5) may be shown to result into the following second order ordinary differential equation after semidiscretization:

$$M_f \ddot{\mathbf{p}} + C_f \dot{\mathbf{p}} + K_f \mathbf{p} = \varrho_f Q_f (\ddot{\mathbf{u}} + \ddot{\mathbf{u}}_g) + \mathbf{f}_f \tag{7}$$

Here M_f, C_f and K_f are the fluid global mass, damping and stiffness matrices respectively. Q_f is the coupling matrix which transfers shell and ground acceleration vectors $\ddot{\mathbf{u}}$ and $\ddot{\mathbf{u}}_g$ respectively to the fluid domain and $\mathbf{f}_f$ is the fluid force vector.

The finite element formulation of the above matrices can be obtained in a straightforward manner by extending the two-dimensional formulation[10,11] as shown by Singh *et al.*[12]. The pressure in the fluid element is given in terms of nodal pressure $\mathbf{p}$ and fluid element shape function N_f as:

$$p = N_f \mathbf{p} \tag{8}$$

The fluid element mass matrix is constituted by impulsive and free surface sloshing terms as:

$$(M_f^e)_{ij} = 1/c^2 \int_{\Omega_f} N_{fi}^{\mathrm{T}} N_{fj} \, \mathrm{d}\Omega_f + 1/g \int_{\Gamma_F} N_{fi}^{\mathrm{T}} N_{fj} \, \mathrm{d}\Gamma_F \tag{9}$$

Fluid element radiation damping matrix is considered for a non-reflecting or radiating boundary Γ_R as:

$$(C_f)^e_{ij} = 1/c \int_{\Gamma_R} N^{\mathrm{T}}_{fi} N_{fj} \, \mathrm{d}\Gamma_R \tag{10}$$

Finally, fluid element stiffness matrix is:

$$(K^e_f)_{ij} = \int_{\Omega_f} (N_{fi,x} N_{fj}, x + N_{fi}, y N_{fj,y} + N_{fi,z} N_{fj,z}) \, \mathrm{d}\Omega_f \tag{11}$$

The coupling matrix Q_f for the fluid domain is given by:

$$(Q_f)_{ij} = \int_{\Gamma_I} N^{\mathrm{T}}_{fi} n_s N_{sj} \, \mathrm{d}\Gamma_I \tag{12}$$

where n_s is the unit normal on the shell surface at the shell–fluid interface.

Coupled shell dynamic analysis

The semidiscrete coupled shell dynamics equation is given by:

$$M_s \ddot{\mathbf{u}} + C_s \dot{\mathbf{u}} + K_s \mathbf{u} = \mathbf{f}_s - M_s \ddot{\mathbf{u}}_g + Q_s \mathbf{p} \tag{13}$$

where M_s, C_s and K_s are the shell global mass, damping and stiffness matrices respectively. $\mathbf{u}$ is the displacement field of the shell structure and a superposed dot denotes differentiation with respect to time, $\mathbf{f}_s$ is the global load vector and $\ddot{\mathbf{u}}_g$ is the specified time history at the base. The addition of the coupling term Q_s in (13) couples this equation with the fluid transient equation (7). It is easily recognized that $Q_s = -Q_f^{\mathrm{T}}$. In code FLUSHEL a nine-noded Lagrangian degenerate shell element with explicit integration through the thickness has been used. The coupling matrices Q_s and Q_f take care of variation in node numbers at the shell–fluid interface. The coupled set of simultaneous equations (7) and (13) are solved in a staggered manner where the transfer of interface data from one field to another field is carried out in sequential manner. In order to economize the storage space, nodal coordinate system is used for the shell dynamics problem. Thus only single variables are associated with Q_s and Q_f which are nodal pressures of the fluid domain and shell normal accelerations of the shell domain respectively. The shell normal accelerations obtained from the solution of shell dynamics equation (13) and fluid pressures obtained from (7) can be directly transferred to the respective interacting fields without any need of further transformation or processing. A separate equation numbering system is evolved at the shell–fluid interface in the skyline solution procedure by keeping only active degrees of freedom (one at each node) at the interface. Finally, the coupling terms in the load vectors are transferred to the original equations of the shell and fluid domains. This scheme requires the minimum computer storage space for the coupling matrices and is very powerful for three-dimensional shell–fluid interaction problems particularly on small computers with inherent limitation on storage space.

Now we define the shell element matrices which are required to obtain the above global matrices. *Figure 1* shows a three-dimensional brick element with a quadratic displacement field description. The shell element is formed by degenerating this element with assumptions of first order shear deformation shell theory. The shell normal stress is neglected and the shell normal is assumed to remain straight after deformation. The shell geometry can be either described by the middle surface nodes and thickness at each node point or by shell top and bottom surface node coordinates. In the present two-dimensional degenerate shell element

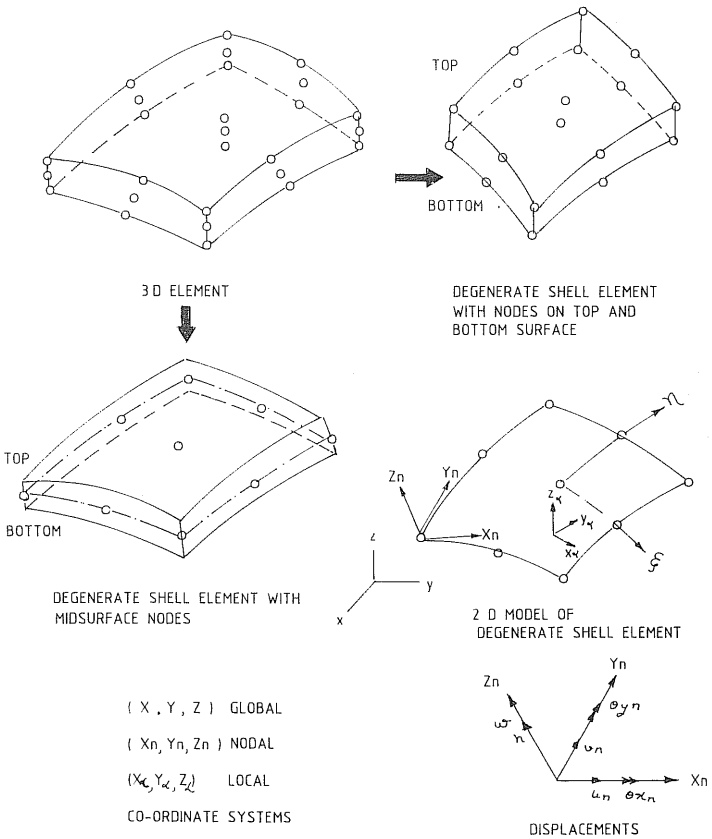

Figure 1 Development of 2D degenerate shell element

formulation explicit integration through the shell thickness leads to definition of three membrane stress resultants Nxx, Nyy and Nxy, three moments Mxx, Myy and Mxy along with two transverse shear resultants Qx and Qy. These are related to corresponding eight strains on the shell middle surface ε_{x0}, ε_{y0}, γ_{xy0}, κ_x, κ_y, κ_{xy}, γ_{xz0} and γ_{yz0}.

This approach is different than the conventional approach[24,28,29] of considering only five strains at any point in the shell body, where either two point gauss integration is carried through the thickness or an individual layer numerical integration approach is followed with one gauss point for each layer. The present approach is economical and more accurate than the conventional approach[23,26]. Three sets of coordinate system (*Figure 1*) are defined namely global (X, Y, Z), nodal (x_n, y_n, z_n) and local $(x_\alpha, y_\alpha, z_\alpha)$ in this formulation. The global coordinate defines the shell geometry, the nodal coordinate defines the nodal displacements and global stiffness, mass and load matrices. The local coordinate is used for numerical integration of element matrices. Nodal and local coordinates are defines by the shell normal vector $\vec{V}_\perp$ at a node n or any α point in the element by:

$$\vec{V}_\perp = \vec{V}_\xi X \vec{V}_\eta \tag{14}$$

where $\vec{V}_\xi$ and $\vec{V}_\eta$ are vectors along ξ and η natural coordinates of the shell element. So once unit normal vector along $\vec{V}_\perp$ ($\vec{k}_n$ at node n and $\vec{k}_\alpha$ at point α within the element) is known, $\vec{i}_n$ or $\vec{i}_\alpha$

for nodal or local coordinates is along $\vec{V}_\xi$ and $\vec{j}_n$ is thus finally defined by:

$$\vec{j}_{n,\alpha} = \vec{k}_{n,\alpha} X \vec{i}_{n,\alpha} \tag{15}$$

The stress and strain resultants are defined in the local coordinate system along with the description of constitutive laws. The global degrees of freedom at a node i in the nodal coordinate system is defined as:

$$\boldsymbol{\delta}_{ni} = [u_{ni}, v_{ni}, w_{ni}, \theta_{xni}, \theta_{yni}]^{\mathrm{T}} \tag{16}$$

The local degrees of freedom in local coordinate system at any node point i in the element is given by:

$$\boldsymbol{\delta}_{\alpha i} = [u_{\alpha i}, v_{\alpha i}, w_{\alpha i}, \theta_{x\alpha i}, \theta_{y\alpha i}]^{\mathrm{T}} \tag{17}$$

where u, v, w are displacement components and θ_x, θ_y are the two rotations respectively. The displacement $\mathbf{u}^e$ in the shell element is defined by:

$$\mathbf{u}^e = \sum_{i=1}^{\text{node}} N_{si} \boldsymbol{\delta}_{ni} \tag{18}$$

where N_{si} is the shape function at node i of the shell element. Strain vector $\boldsymbol{\varepsilon}_\alpha$ at a point α in the element is given in terms of local displacements as:

$$\boldsymbol{\varepsilon}_\alpha = \sum_{i=1}^{\text{node}} \mathbf{B}_i \boldsymbol{\delta}_{\alpha i} \tag{19}$$

and

$$\boldsymbol{\delta}_{\alpha i} = \mathbf{R}_{\alpha i} \boldsymbol{\delta}_{ni} \tag{20}$$

where $\mathbf{R}_{\alpha i}$ is the transformation matrix relating local displacement to nodal displacement and $\mathbf{B}_i$ is the strain displacement matrix at any node i. Thus we have:

$$\boldsymbol{\varepsilon}_\alpha = \sum_{i=1}^{\text{node}} \mathbf{B}_i^* \boldsymbol{\delta}_{ni} \tag{21}$$

where

$$\mathbf{B}_i^* = \mathbf{B}_i \mathbf{R}_{\alpha i} \tag{22}$$

For the shell element $\mathbf{B}^*$ matrix can be defined by augmenting contributions from all the nodes of the element as:

$$\mathbf{B}^* = [\mathbf{B}_1^*, \mathbf{B}_2^*, \ldots, \mathbf{B}_i^*, \ldots, \mathbf{B}_n^*] \tag{23}$$

The shell element stiffness matrix is defined as:

$$(\mathbf{K}_s^e)_{ij} = \int_{As} \mathbf{B}_{im}^{*\mathrm{T}} \mathbf{D}_{mk} \mathbf{B}_{kj}^* t \, \mathrm{d}A_s \tag{24}$$

where $\mathbf{D}$ is the elasticity matrix relating mid-surface stress resultants to the strains and t is the thickness of the shell. The element mass matrix with density ϱ_s is:

$$(\mathbf{M}_s^e)_{ij} = \int_{As} \varrho_s \mathbf{N}_{si}^{\mathrm{T}} \mathbf{N}_{sj} \int_{As} \varrho_s \mathbf{N}_{si}^{\mathrm{T}} \mathbf{N}_{sj} t \, \mathrm{d}A_s \tag{25}$$

Special mass lumping is employed for the translational degrees of freedom as shown by Hinton *et al.*[35], while for the rotational degrees of freedom the terms are normalized by $m_i t_i^2/4$. This normalization is based on a scheme proposed by Surana[36] for degenerate C^0 continuous shell

elements. Here m_i and t_i are mass and thickness at node i respectively. The element stiffness matrix is evaluated by selective integration scheme with 2×2 reduced integration for shear and membrane terms while 3×3 full integration is used for bending terms. The structure damping matrix is constructed by:

$$\mathbf{C}_s = a\mathbf{M}_s + b\mathbf{K}_s \tag{26}$$

where constants a and b can be chosen suitably to control damping proportionately.

TIME INTEGRATION OF COUPLED FIELD EQUATIONS

The set of coupled equations (7) and (13) are solved by the method of partitioning. Hughe's predictor multicorrector integration scheme has been shown to be very powerful for such coupled problems by Paul[10] and Singh *et al.*[11,12]. The interaction between the two fields is studied in a staggered manner by transferring field variables from one field to another field. This time integration scheme has been derived by combining implicit and explicit integration schemes of Newark's method in predictor/multi-corrector form. Here the elements are recognized as either implicit or explicit. There could be two possible paths for coupled problems. In the first case the predicted fluid variable is transferred to the structure and the corrected structure response after the solution of system of structure equations, is transferred to the fluid domain. Alternatively, the second path could be just opposite to this, where the predicted structure variable is transferred to the fluid domain at first and then corrected fluid responses could be transferred to the structure domain. Singh *et al.*[11] have compared the two paths and it has been established that the second path is suitable for problems of wave propagation in fluid, where a pressure pulse in fluid moves and transfers load on the structure, while the first path is suitable for problems of structural motion induced oscillations in fluid such as in the case of storage tanks, reservoirs etc. For the present submerged shell problems thus, the second path leads to rapid convergence.

For coupled shell fluid dynamic problems the shell domain is normally very stiff compared to the fluid domain. So the fluid field should normally be discretized with explicit elements while the shell field should be discretized by implicit elements. This is very advantageous since normally the fluid field is of quite large size, and explicit description results into economical analysis with optimum storage space and CPU time in the computer. The present formulation with quadratic displacement field description for shell domain and linear pressure field description for the fluid domain is very powerful. Here the nodal spacing in the fluid domain is twice that of the shell domain, which allows above type of explicit–implicit partitioning for fluid and shell meshes more conveniently.

The integration scheme reported earlier[10,11,22,29] is given below in brief. We consider a set of second order equations at time step $n+1$ as:

$$\mathbf{M}\ddot{\mathbf{u}}_{n+1} + \mathbf{C}\dot{\mathbf{u}}_{n+1} + \mathbf{K}\mathbf{u}_{n+1} = \mathbf{F}_{n+1} \tag{27}$$

Here the subscript in the coefficient matrices has been dropped as it may be used for any field. The force term augments applied force, specified boundary conditions and interaction term from other fields. In the predictor phase the field variables are expressed as:

$$\mathbf{u}^i_{n+1} = \tilde{\mathbf{u}}_{n+1} \tag{28}$$

$$\dot{\mathbf{u}}^i_{n+1} = \tilde{\dot{\mathbf{u}}}_{n+1} \tag{29}$$

$$\ddot{\mathbf{u}}^i_{n+1} = \mathbf{0} \tag{30}$$

where i is the iteration count and

$$\tilde{\dot{\mathbf{u}}}_{n+1} = \dot{\mathbf{u}}_n + \Delta t(1-\gamma)\ddot{\mathbf{u}}_n \tag{31}$$

$$\tilde{\mathbf{u}}_{n+1} = \mathbf{u}_n + \Delta t\dot{\mathbf{u}}_n + 1/2\Delta t^2(1-2\beta)\ddot{\mathbf{u}}_n \tag{32}$$

Here γ and β are Newmark's parameters, Δt is the time step.

In the solution phase the following equation is formed and solved:

$$\mathbf{K}^*\Delta\mathbf{u}^i = \mathbf{f}^{*i}_{n+1} \tag{33}$$

where

$$\mathbf{K}^* = \mathbf{M}/\beta\,\Delta t^2 + \gamma\mathbf{C}/\beta\,\Delta t + \mathbf{K} \tag{34}$$

and

$$\mathbf{f}^{*i}_{n+1} = \mathbf{F}^i_{n+1} - \mathbf{M}\ddot{\mathbf{u}}^i_{n+1} - \mathbf{C}\dot{\mathbf{u}}^i_{n+1} - \mathbf{K}\mathbf{u}^i_{n+1} \tag{35}$$

Once the increment in field variable is obtained, field variables are updated as follows:

$$\mathbf{u}^{i+1}_{n+1} = \mathbf{u}^i_{n+1} + \Delta\mathbf{u}^i \tag{36}$$

$$\ddot{\mathbf{u}}^{i+1}_{n+1} = (\mathbf{u}^{i+1}_{n+1} - \tilde{\mathbf{u}}_{n+1})/\beta\,\Delta t^2 \tag{37}$$

$$\dot{\mathbf{u}}^{i+1}_{n+1} = \dot{\mathbf{u}}^i_{n+1} + \gamma\Delta t\ddot{\mathbf{u}}^{i+1}_{n+1} \tag{38}$$

Finally, a convergence check is made on the norm of increment in field variable compared to the norm of total field variable as:

Is $\|\Delta\mathbf{u}^i\|/\|\mathbf{u}^{i+1}\| \leqslant e$ (the specified tolerance) ? (39)

$i \rightarrow i+1 \leftarrow$ NO
and go to (33)
for next iteration

YES
$n \rightarrow n+1$
and go to (27) for next time step

Element wise mesh partitioning is done by recognizing elements as explicit or as implicit,

$$\mathbf{M} = \mathbf{M}^I + \mathbf{M}^E \tag{40}$$

$$\mathbf{C} = \mathbf{C}^I + \mathbf{C}^E \tag{41}$$

$$\mathbf{K} = \mathbf{K}^I + \mathbf{K}^E \tag{42}$$

$$\mathbf{F} = \mathbf{F}^I + \mathbf{F}^E \tag{43}$$

and modifying the governing equation (27) as:

$$\mathbf{M}^I\ddot{\mathbf{u}}_{n+1} + \mathbf{M}^E\ddot{\mathbf{u}}_{n+1} + \mathbf{C}^I\dot{\mathbf{u}}_{n+1} + \mathbf{K}^I\mathbf{u}_{n+1} = \mathbf{F}^I_{n+1} + \mathbf{F}^E_{n+1} \tag{44}$$

The stability criteria of Newmark's integrator for single field with single pass is well established[22,28,30,32]. $\gamma \geqslant 1/2$ and $\beta = (\gamma + 1/2)^2/4$ lead to unconditional stability.

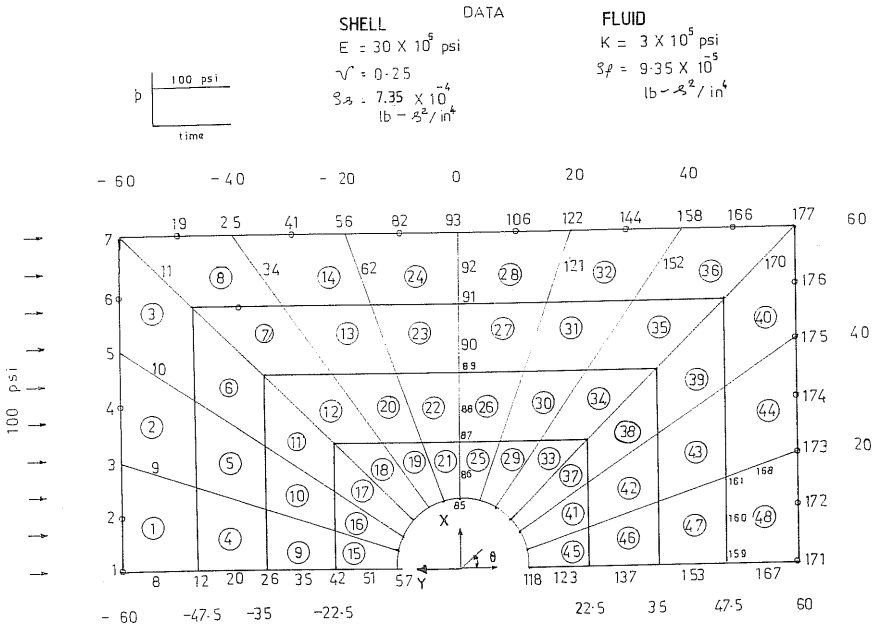

Figure 2 Single submerged cylindrical shell in infinite fluid

SINGLE SUBMERGED CYLINDRICAL TUBE PROBLEM

Plane strain analysis with two-dimensional code FLUSOL

Figure 2 shows a long submerged cylindrical tube subjected to a fluid pulse of 100 lb/in^2 applied from the left end while the other boundaries are fixed. This problem has been studied by Paul[10] using displacement potential function formulation for fluid domain with two-dimensional plane strain assumptions. Two-dimensional transient analysis of this problem with 8-noded isoparametric continuum elements was conducted by code FLUSOL[11] developed by the present authors, which is based on pressure formulation for the fluid domain and displacement formulation for the structural domain. *Figure 3a* shows the horizontal velocity response of the shell at $\theta=\pi/2$ and $\theta=0$ (rear edge) at a time step of 10^{-5} sec (same as in Reference 10) with explicit fluid, implicit structure mesh descriptions along with implicit fluid, implicit structure mesh descriptions. Good agreement is noted with the results reported in the reference. Further study was conducted by applying radiation boundary condition at $Y=-60$ in and $X=60$ in, to represent the case of an infinite acoustic medium. Exact analytical and numerical boundary element results are available in terms of non-dimensional radial velocity response $\varrho_f C\dot{w}/PI$ and time parameter ct/a due to Geers[37,38]. Here $\dot{w}$ is the radial velocity and PI is the incident pulse intensity (100 lb/in^2 in this case), a is the cylinder radius and t is the time.

Eigen value analysis of the mesh in *Figure 2* gives the critical time steps of 1.6×10^{-7} sec for the cylindrical shell structure and 2.05×10^{-5} sec for the fluid domain. A time step of 1.75×10^{-5} sec was selected for the analysis along with implicit description of the structure mesh. *Figure 3b* shows the radial velocity response at the front edge ($\theta=\pi$) and the rear edge ($\theta=0$) of the cylindrical shell. In this case the results are given for explicit–implicit (E–I) and implicit–implicit (I–I) partitionings of the fluid and structure meshes respectively. Both consistent and lumped radiation damping matrices have been used in the former case. *Figure 3c* shows the

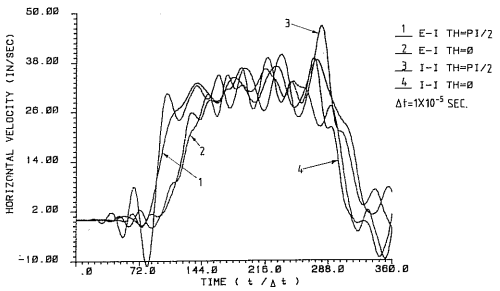

Figure 3a Submerged cylinder with fluid pulse

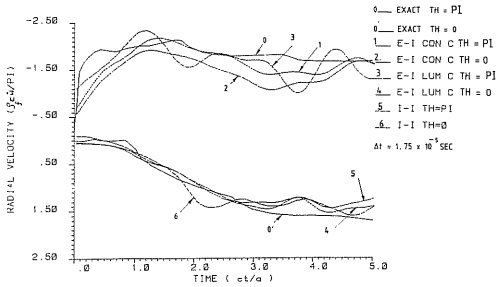

Figure 3b Submerged cylinder in infinite fluid

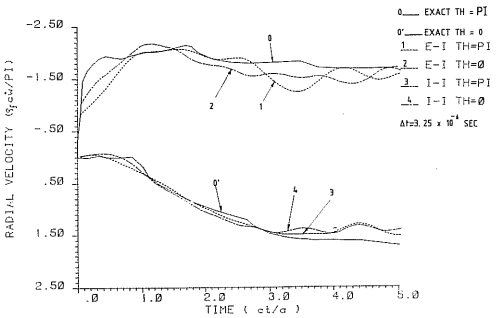

Figure 3c Submerged cylinder in infinite fluid

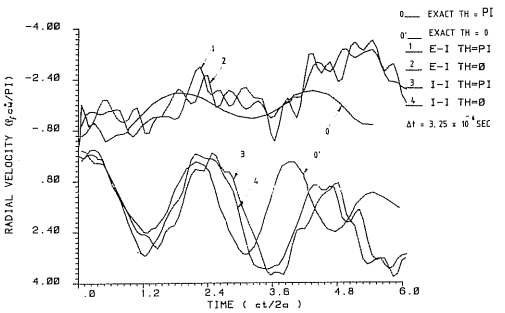

Figure 3d Submerged sphere in infinite fluid

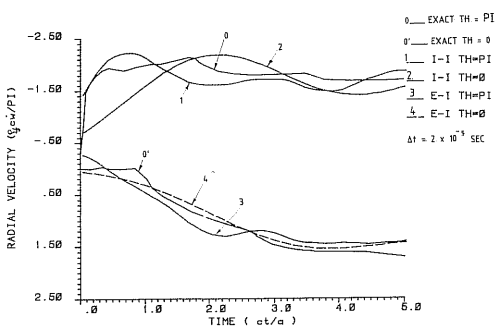

Figure 4a Submerged cylinder in infinite fluid (P/S)

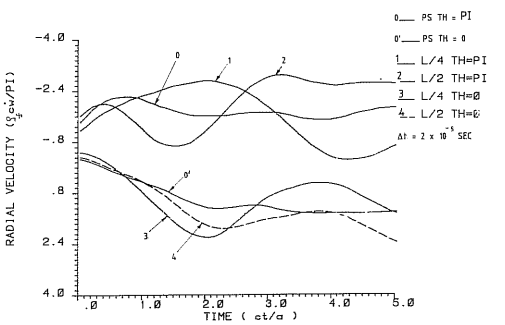

Figure 4b Submerged cylinder in infinite fluid (SSSUW)

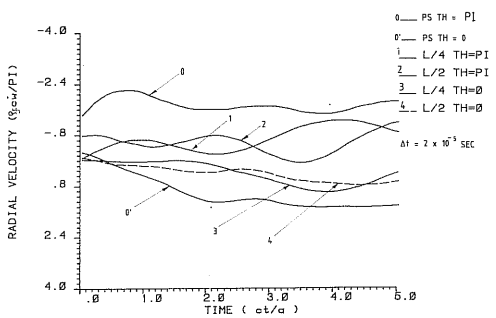

Figure 4c Submerged cylinder in infinite fluid (SSLIW)

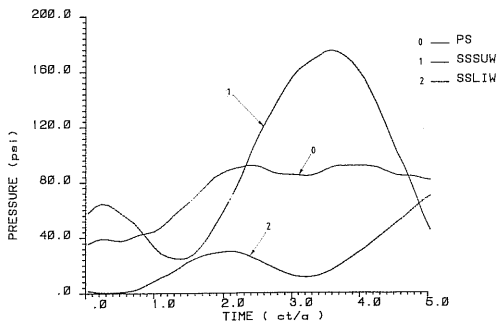

Figure 5 Pressure history ($L/4$ theta = PI) single cylinder

results for a finer mesh and good convergence is noted with respect to the mesh refinement. In this case the critical time steps for structure and fluid meshes were 8×10^{-8} and 3.9×10^{-6} sec respectively. Again implicit description of the structure is desirable from the point of view of minimum CPU time. A time step of 3.25×10^{-6} sec was used for the analysis in this case. The same meshes were used to study the case of a submerged sphere in an infinite fluid medium with axisymmetric continuum elements. The first mesh gave very poor results, while the refined mesh gave results to an acceptable accuracy level which are shown in *Figure 3d*. It may be noted that the rate of increase in scattering area with respect to the wave propagation direction in spherical shell is larger than the cylindrical shell, hence a more refined mesh is required in the former case.

Three-dimensional response with code FLUSHEL

Figure 4a shows the radial velocity response obtained by three-dimensional analysis with code FLUSHEL[12]. In this case the 9-noded Lagrangian degenerate shell elements have been used for the tube along with 8-noded trilinear elements to represent the fluid domain. Two elements have been taken across the cylinder axis for the shell and the fluid meshes. Shell edges are constrained to obtain a plane strain solution (case PS). Again good agreement is noted with the reported results[38], for *E–I* and *I–I* mesh partitionings of the fluid and shell meshes. As mentioned earlier the present interest is to obtain the three-dimensional solution of the submerged cylindrical tube, hence one edge of the cylindrical tube was simply supported without any axial restraint while symmetry condition was applied at the other end. The eigen value analysis shows that the dry tube has the fundamental frequency of 68.8 Hz in the first axial ($m=1$) and third circumferential ($n=3$) mode. Two loadings are considered, one with a uniform surface wave of 100 lb/in^2 (case SSSUW) along the full span and the other with a line wave of 100 lb/in^2 (case SSLIW) at the mid span applied from the left end (*Figure 2*). The radial velocity response of the simply supported tube for the case SSSUW is shown in *Figure 4b* where the results of plane strain (case PS) are also shown for comparison purpose. It is noted that the velocity response in this case is significantly higher than the plane strain solution (case PS) due to inclusion of bending mode and presence of three dimensional fluid field. *Figure 4c* shows the radial velocity response for the case SSLIW where the tube is simply supported and is subjected to a line wave. In this case although the velocity is lower than SSSUW case due to lower value of net load on the tube, the dynamic behaviour of the tube is different than that given by case PS. *Figure 5* compares the pressure responses for cases PS, SSSUW and SSLIW at the front edge ($\theta=\pi$) of quarter span ($L/4$). Again it is noticed that the 3-D pressure response is higher for surface wave loading compared to the plane strain solution. For the line wave loading the pressure is significantly lower than the plane strain case which is consistent with the velocity response. *Figure 6a* shows the axial membrane force (Nxx) at four locations namely at the front edge of quarter span ($\theta=\pi$, $L/4$), at the front edge of mid span ($\theta=\pi$, $L/2$), at the rear edge of quarter span ($\theta=0$, $L/4$) and at the rear edge of mid span ($\theta=0$, $L/2$) for SSSUW case along with PS case for comparison purpose. It is apparent that 3-D solution shows significant increase in response. Similar trend is noted for circumferential membrane force (Nyy) in *Figure 6b*. *Figure 6c* shows the axial moment (Mxx) at the above mentioned locations for SSSUW case along with PS case. It is noted that the 3-D solution shows significant bending response which is not shown by the PS solution. Similarly the circumferential moment (Myy) obtained by 3-D analysis is seen to be higher than that obtained by PS solution in *Figure 6d*.

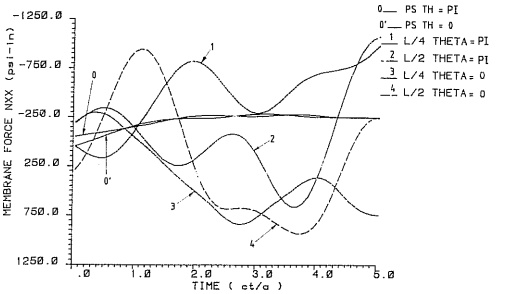

Figure 6a Membrane force *Nxx* in single cylinder (SSSSUW)

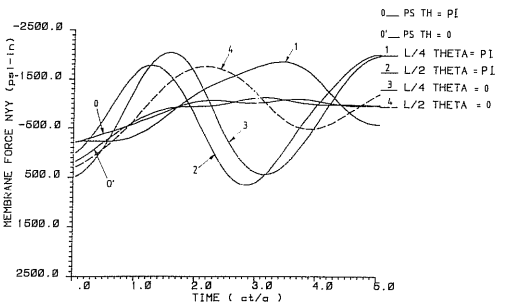

Figure 6b Membrane force *Nyy* in single cylinder (SSSUW)

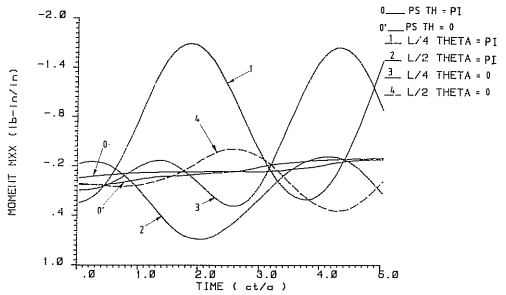

Figure 6c Moment *Mxx* in single cylinder (SSSUW)

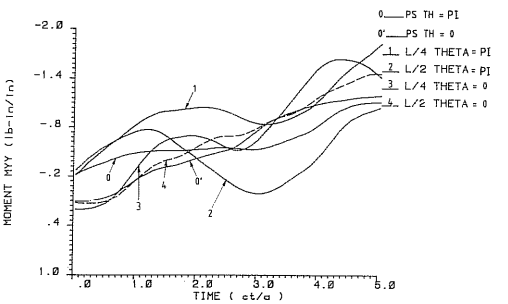

Figure 6d Moment *Myy* in single cylinder (SSSUW)

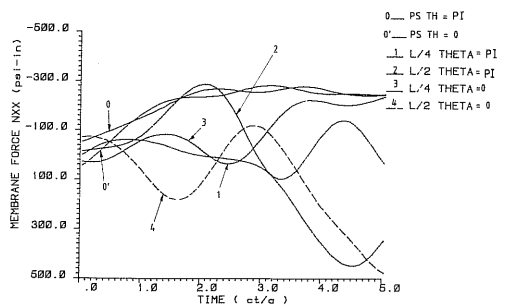

Figure 6e Membrane force *Nxx* in single cylinder (SSLIW)

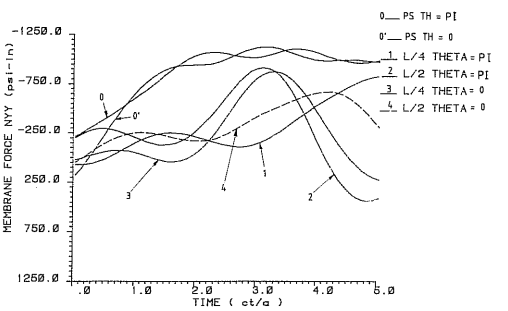

Figure 6f Membrane force *Nyy* in single cylinder (SSLIW)

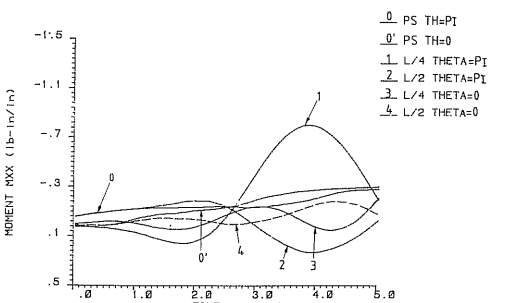

Figure 6g Moment *Mxx* in single cylinder (SSLIW)

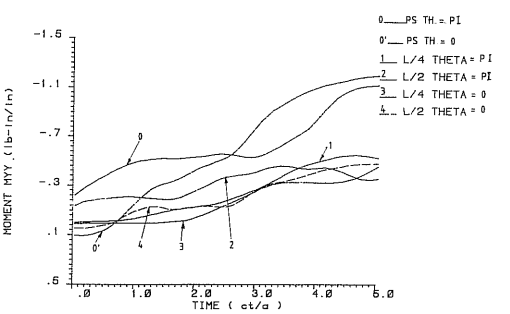

Figure 6h Moment *Myy* in single cylinder (SSLIW)

Next we consider the case of line wave loading on the simply supported submerged tube (case SSLIW). *Figures 6e* and *6f* show the axial membrane force (Nxx) and circumferential membrane force (Nyy) respectively at the four locations along with PS solution. It is noticed that the circumferential membrane force (Nyy) is less than that indicated by PS solution due to lower value of the net load on the tube which is consistent with the radial velocity response. However, for the present case the axial membrane force (Nxx) is higher than the PS solution. *Figures 6g* and *6h* compare the axial and circumferential moments (Mxx and Myy) for SSLIW case along with PS case. Here it is noticed that the circumferential moment (Myy) is lower than PS solution while the axial moment (Mxx) is shown to be significant which is ignored in the case of two-dimensional solution (PS). The three-dimensional analysis shows that for a line wave loading there is significant increase in axial membrane force (Nxx) at rear edge of tube mid span (*Figure 6e*) and axial moment (Mxx) at the front edge of the tube (*Figure 6g*). This is due to increase in pressure response on the rear edge of mid span which results due to inclusion of bending mode along with three-dimensional variation in pressure field. This is further examined in detail for the next problem.

Now we consider the case of a cylindrical tube held at the ends with axial constraint since this case is of practical interest in the area of heat exchanger design. Two types of boundary conditions are considered, one of a simply supported tube with full axial constraint and another of a clamped tube. Again both types of loadings are considered. Thus we have a total of four cases namely, (i) simply supported tube with axial restraint and loaded with a uniform surface wave of 100 lb/in^2 along the full span (case SSASUW), (ii) simply supported tube with axial restraint and loaded with a line wave of 100 lb/in^2 at the tube centre (case SSALIW), (iii) clamped tube loaded by a uniform surface wave of 100 lb/in^2 on the full span (case CLSUW), (iv) clamped tube loaded by a line wave of 100 lb/in^2 at the tube centre (case CLLIW). In the simple support condition with axial constraint the tube has the fundamental frequency of 86.4 Hz again in the first axial ($m=1$) and third circumferential ($n=3$) mode. For the clamped tube the fundamental frequency is 86.8 Hz in the same mode. *Figure 7a* compares the radial velocity response at the front and rear edges at the earlier mentioned locations of quarter span and mid span for SSASUW case with PS case. Again effect of bending is noticed and the response increases compared to the PS solution. In case of line wave loading case SSALIW, the radial velocity response is lower than PS solution as shown in *Figure 7b*. In case of clamped tube (*Figures 7c* and *7d*) similar behaviour is noticed for the two types of waves (cases CLSUW and CLLIW). It is also noticed that the mid span radial velocity is more than the quarter span velocity and in the clamped tube case the radial velocities are slightly higher than the simply supported tube cases.

Figures 8a and *8b* compare the pressure history at various locations of the tube for SSASUW case and CLSUW case respectively. It is noticed that the pressure is the maximum at the front edge of mid span ($\theta=\pi$, $L/2$) and it is only slightly more for the clamped tube case compared to the simply supported tube case. The pressure is also significant at the rear edge of mid span ($\theta=0$, $L/2$) for the clamped tube case compared to the case of simply supported tube. This justifies the higher response in case of CLSUW compared to SSASUW case. Comparison of the three cases SSSUW, SSASUW and CLSUW demonstrates that as the tube stiffness increases it offers more resistance to the wave which results in higher induced pressure and velocity fields of the tube. Similar behaviour is noticed in the case of line wave loading in *Figures 8c* and *8d*.

Figures 9a–9d show the axial membrane force (Nxx) at the four locations for SSASUW, SSALIW, CLSUW and CLLIW cases along with case PS for comparison purpose. Again it is noticed that for the surface wave loading the response is higher than the PS case, mid span membrane force is more than that at the quarter span and the clamped tube gives axial membrane force slightly higher than the simply supported axially constrained tube case. At the rear edge

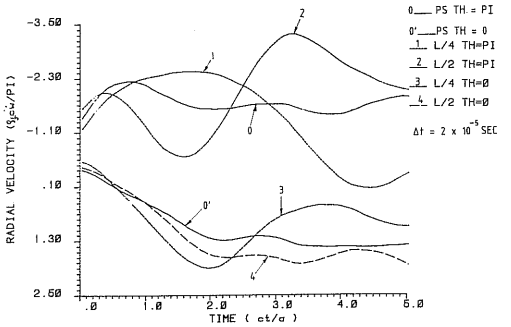

Figure 7a Submerged cylinder in infinite fluid (SSASUW)

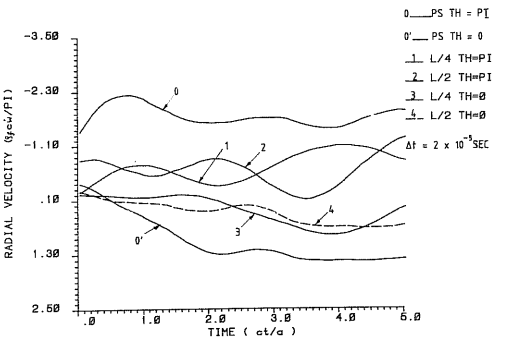

Figure 7b Submerged cylinder in infinite fluid (SSALIW)

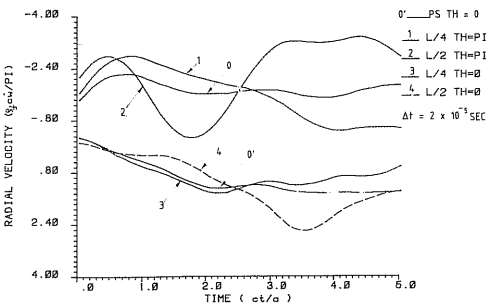

Figure 7c Submerged cylinder in infinite fluid (CLSUW)

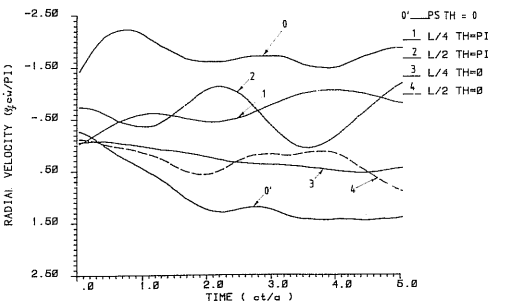

Figure 7d Submerged cylinder in infinite fluid (CLLIW)

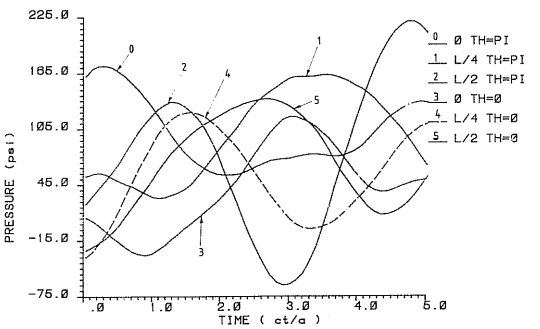

Figure 8a Pressure history in single cylinder (SSASUW)

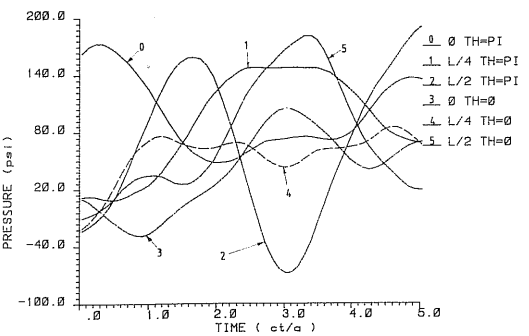

Figure 8b Pressure history in single cylinder (CLSUW)

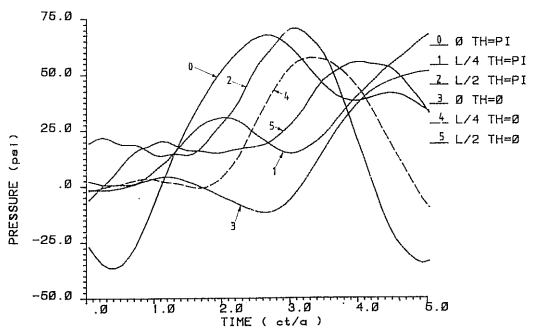

Figure 8c Pressure history in single cylinder (SSALIW)

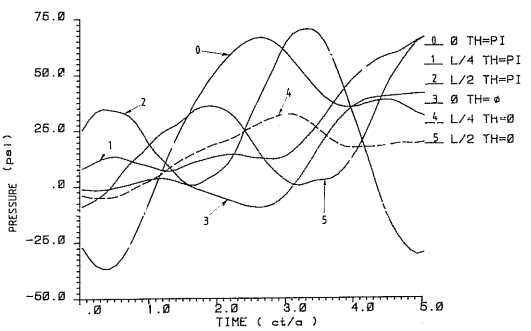

Figure 8d Pressure history in single cylinder (CLLIW)

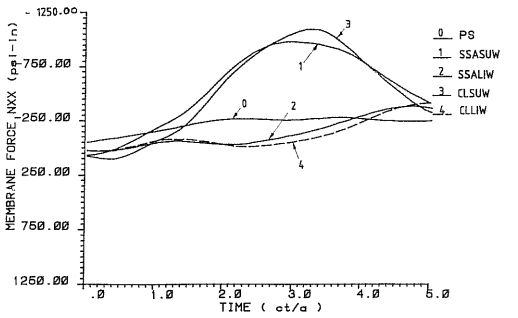

Figure 9a Nxx at node 3 ($L/4$ theta = PI) single cylinder

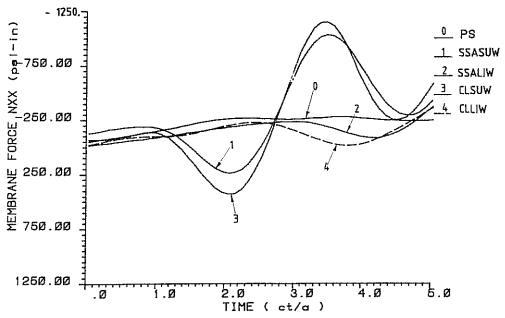

Figure 9b Nxx at node 5 ($L/2$ theta = PI) single cylinder

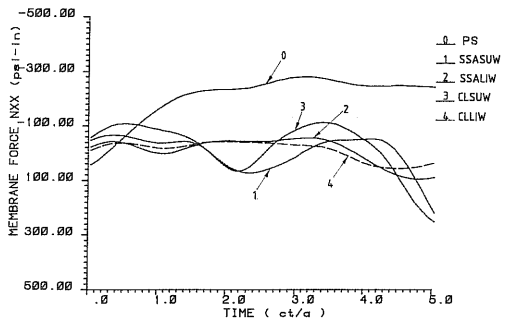

Figure 9c Nxx at node 123 ($L/4$ theta = 0) single cylinder

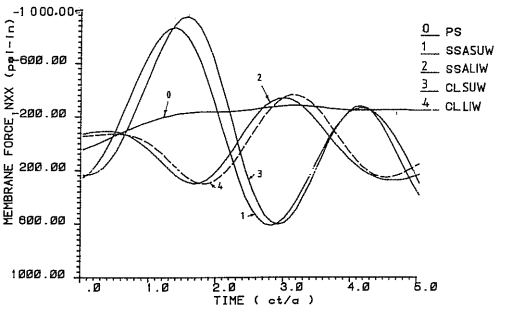

Figure 9d Nxx at node 125 ($L/2$ theta = 0) single cylinder

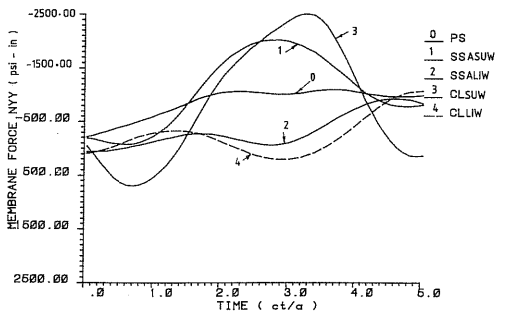

Figure 10a Nyy at node 3 ($L/4$ theta = PI) single cylinder

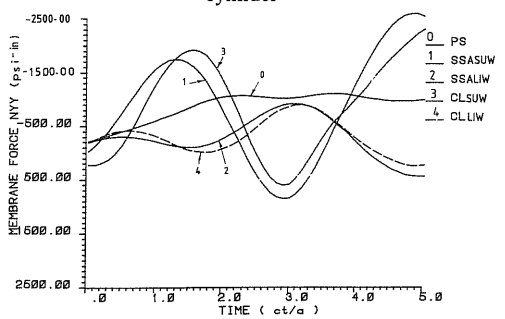

Figure 10b Nyy at node 5 ($L/2$ theta = PI) single cylinder

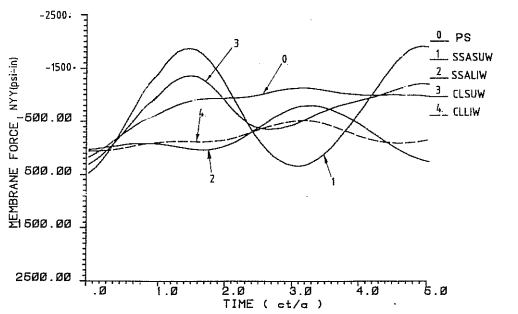

Figure 10c Nyy at node 123 ($L/4$ theta = 0) single cylinder

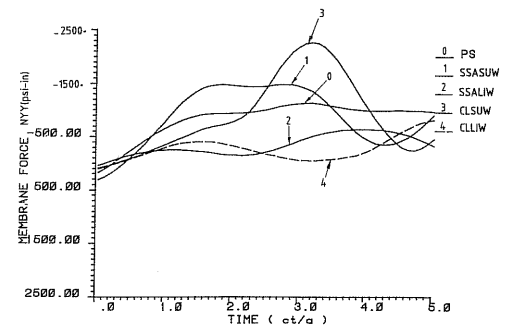

Figure 10d Nyy at node 125 ($L/2$ theta = 0) single cylinder

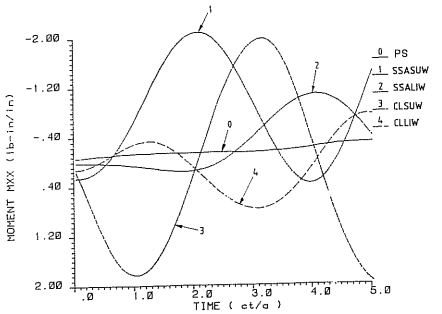

Figure 11a *Mxx* at node 3 (*L*/4 theta = PI) single cylinder

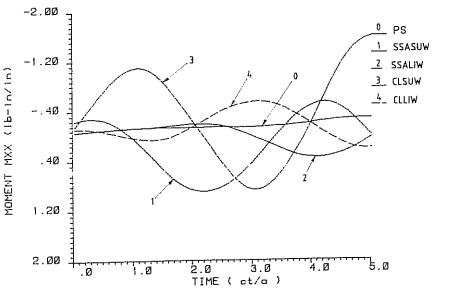

Figure 11b *Mxx* at node 5 (*L*/2 theta = PI) single cylinder

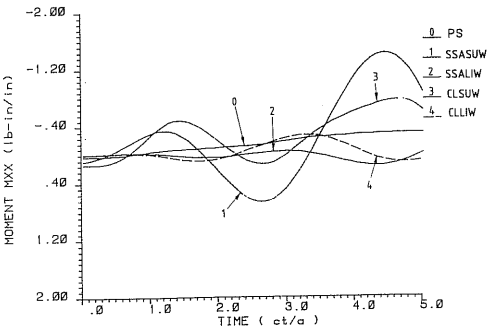

Figure 11c *Mxx* at node 123 (*L*/4 theta = 0) single cylinder

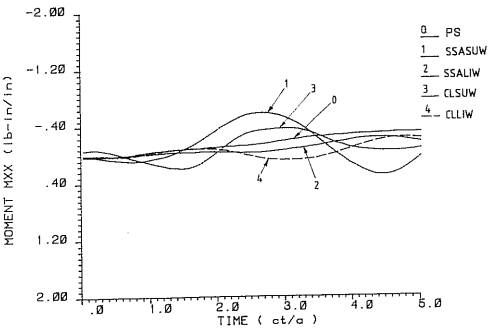

Figure 11d *Mxx* at node 125 (*L*/2 theta = 0) single cylinder

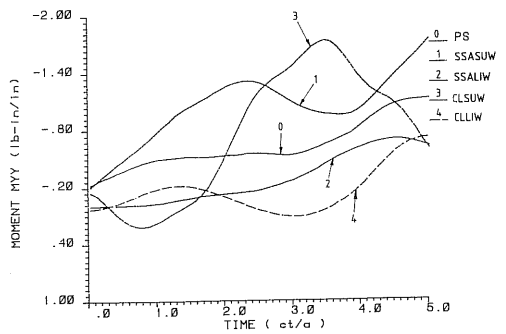

Figure 12a *Myy* at node 3 (*L*/4 theta = PI) single cylinder

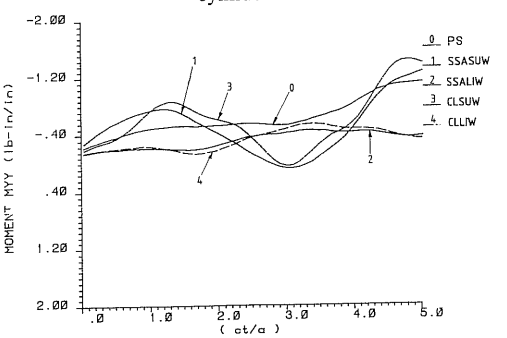

Figure 12b *Myy* at node 5 (*L*/2 theta = PI) single cylinder

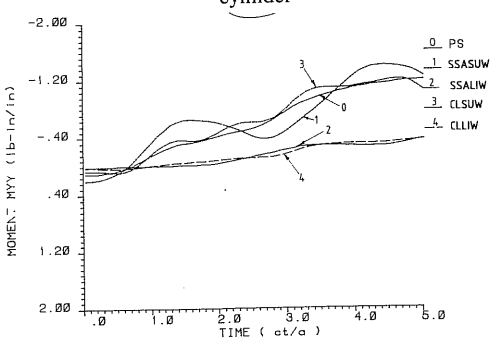

Figure 12c *Myy* at node 123 (*L*/4 theta = 0) single cylinder

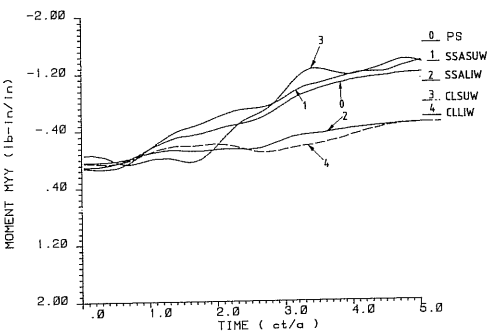

Figure 12d *Myy* at node 125 (*L*/2 theta = 0) single cylinder

of the mid span even the line wave loading results into higher axial membrane force than that of case PS. Similar behaviour is noticed for the circumferential membrane force (Nyy) in *Figures 10a–10d* with the only exception at the quarter span of the rear edge where the clamped tube response is lower than the simply supported tube response. *Figures 11a–11d* show the axial moment (Mxx) for the above-mentioned cases. Again it is noticed that there is significant axial bending moment which is normally not associated with the simple two-dimensional solution. In this case the quarter span moment is more than the corresponding mid span value indicating that higher modes are also excited significantly. Circumferential moment (Myy) is shown in *Figures 12a–12d*. In this case also the surface wave loading results into higher moment compared to PS solution while the line wave loading gives a lower circumferential moment compared to PS solution and the maximum response is at the quarter span of the front edge.

In the three-dimensional analysis of single submerged cylindrical tube presented in this paper, the critical time steps for fluid and shell meshes are 3×10^{-5} and 5.9×10^{-7} sec respectively. This suggests that a practical analysis is possible with implicit description of the shell mesh, while the fluid mesh could be integrated with an explicit integrator. Experience shows that the time step should be slightly lower (~ 20 to 25%) than the critical time step of fluid mesh[11,12] for such partitioning. The reason for this is that the interaction term appears as a perturbation which may be considered analogous to a pseudo non-linear term of non-linear dynamics problem[4]. Initial trials with time steps of 2.75×10^{-5} and 2.5×10^{-5} sec resulted in a very large number of iterations per time step. One possible reason for this is that the tube has the fundamental frequency of 68.8 Hz in SSSUW case with $m=1$ and $n=3$ mode; however, response of the tube indicates that combination of modes $m=1$ and $m=2$ along with $n=1$ is the predominant which corresponds to frequencies of 183 Hz and 733 Hz respectively. Thus a practical time step of 2×10^{-5} sec was selected to include significant modes of tube vibration in the analysis. The selection of time step is thus dependent on the critical time steps for the fluid and structure meshes along with the modes of excitation for such coupled three-dimensional transient problems.

CONCLUSIONS

In the present paper a practical methodology to analyse coupled three-dimensional fluid–structure interaction problems has been presented. The two-dimensional degenerate shell element with explicit through thickness integration can be effectively coupled with a three-dimensional trilinear fluid element for transient analysis. Effective explicit–implicit partitioning is achieved for shell and fluid meshes in an optimum manner by using a staggered solution scheme. The three-dimensional transient analysis of a single submerged tube presented in this paper demonstrates the importance of the bending mode along with the three-dimensional variation in fluid field for surface wave and line wave loadings. This is an important aspect of submerged tube design which requires attention by designers. Simplified two-dimensional plane strain solution does not necessarily give out conservative results, thus a three-dimensional transient analysis is necessary for such submerged structures and components.

REFERENCES

1 Bathe, K. J. and Hahn, W. F. On transient analysis of fluid–structure systems, *Comp. Struct.* **10**, 383–391 (1979)
2 Liu, W. K. and Chang, H. G. A method of computation for fluid structure interaction, *Comp. Struct.* **20**, 311–320 (1985)
3 Liu, W. K. Development of finite element procedures for fluid structures interaction, *PhD Thesis*, EERL 80–86, Cal. Tech./Univ. of Cal., Berkeley (1981)
4 Belytschko, T. Fluid–structure interaction, *Comp. Struct.*, **12**, 459–469 (1980)

5 Akkas, N., Akay, H. U. and Yilmaz, C. Applicability of general purpose finite element programmes in solid–fluid interaction problems, *Comp. Struct.*, **10**, 773–783 (1979)
6 Wilson, E. L. and Khalvati, M. Finite elements for the dynamic analysis of fluid–solid systems, *Int. J. Num. Meth. Eng.*, **19**, 1657–1668 (1983)
7 Shantaram, D., Owen, D. R. J. and Zienkiewicz, O. C. Dynamic transient behaviour of two or three-dimensional structures, including plasticity, large deformation effects and fluid interaction, *Earthq. Eng. Struct. Dyn.*, **4**, 561–576 (1976)
8 Deshpande, S. S., Belkune, R. M. and Ramesh, C. K. Dynamic analysis of coupled fluid–structure interaction problems, *Numerical Methods for Coupled Problems* (Eds. Hinton, E., Bettess, P. and Lewis, R. W.), Pineridge Press, Swansea, 367–378 (1981)
9 Au-Yang, M. K. and Galford, J. E., Fluid–structure interaction—a survey with emphasis on its application to nuclear steam system design, *Nucl. Eng. Des.*, **70**, 387–399 (1982)
10 Paul, D. K. Single and coupled multifield problems, *PhD Thesis*, University College of Swansea, University of Wales (1982)
11 Singh, R. K., Kant, T. and Kakodkar, A. Efficient partitioning schemes for fluid–structure interaction problems, *Eng. Comput.*, **7**, 101–115 (1990)
12 Singh, R. K., Kant, T. and Kakodkar, A. Studies of shell fluid interaction problems., *Proc. Int. Conf. Eng. Software* (*ICENSOFT '89*) (Eds. C. V. Ramakrishnan, A. Varadrajan and C. S. Desai), Narosa, New Delhi (1989)
13 Blevins, R. D. *Flow Induced Vibration*, Van Nostrand/Reinhold, New York (1977)
14 Chen, S. S. *Flow Induced Vibration of Circular Cylindrical Structures*, Hemisphere, Washington, DC (1987)
15 Au-Yang, M. K. Dynamics of coupled fluid-shells, *ASME J. Vib. Stress Reliability Design*, **108**, 339–347 (1986)
16 Dong, R. G. Effective mass and damping of submerged structures, *UCRL—52342*, Lawrence Livermore Laboratory, Univ. of California (1978)
17 Park, K. C. and Felippa, C. A. Partitioned analysis of coupled systems, *Computational Methods for Transient Analysis* (Eds. Belytschko, T. and Hughes, T. J. R.), Ch. 3, Elsevier, Amsterdam (1983)
18 Felippa, C. A. and Geers, T. L. Partitioned analysis for coupled mechanical systems, *Eng. Comput.*, **5**, 123–133 (1988)
19 Zienkiewicz, O. C. and Newton, R. E. Coupled vibrations of a structure submerged in a compressible fluid, *Proc. Int. Symp. Finite Element Techniques* (Ed. M. Sorensen), Univ. of Stuttgart (1969)
20 Zienkiewicz, O. C. and Bettess, P. Fluid–structure dynamic interactions and wave forces—an introduction to numerical treatment, *Int. J. Num. Meth. Eng.* **13**, 1–16 (1978)
21 Ahmad, S., Irons, B. M. and Zienkiewicz, O. C. Analysis of thick and thin shell structures by curved elements, *Int. J. Num. Meth. Eng*, **2**, 419–451 (1970)
22 Hughes, T. J. R. *The Finite Element Method*, Prentice-Hall, Englewood Cliffs, NJ (1987)
23 Belytschko, T. Stress projection for membrane and shear locking in shell finite elements, *Comp. Meth. Appl. Mech. Eng.*, **51**, 221–258 (1985)
24 Hinton, E. and Owen, D. R. J. *Finite Element Software for Plates and Shells*, Pineridge Press, Swansea (1984)
25 Pugh, E. D. L., Hinton, E. and Zienkiewicz, O. C. A study of quadrilateral plate bending elements with reduced integration, *Int. J. Num. Meth. Eng.*, **12**, 1059–1079 (1978)
26 Milford, R. V. and Schnobrich, W. C. Degenerated isoparametric finite elements using explicit integration, *Int. J. Num. Meth. Eng.*, **23**, 133–154 (1986)
27 Owen, D. R. J. and Filho, J. S. R. Alves, Using transputers in finite element computations, *Proc. Int. Conf. Eng. Software* (*ICENSOFT '89*) (Eds. C. V. Ramakrishnan, A. Varadrajan and C. S. Desai), Narosa, New Delhi (1989)
28 Zienkiewicz, O. C., *The Finite Element Method*, 3rd edn McGraw-Hill, London (1976)
29 Owen, D. R. J. and Hinton, E. *Finite Elements in Plasticity: Theory and Practice*, Pineridge Press, Swansea (1980)
30 Belytschko, T. and Hughes, T. J. R.(Eds), *Computational Methods for Transient Analysis*, Elsevier, Amsterdam (1983)
31 Belytschko, T. A survey of numerical methods and computer programmes for dynamic structural analysis, *Nucl. Eng. Des.*, **37**, 23–24 (1976)
32 Belytschko, T. and Mullen, R., Stability and explicit–implicit mesh partitions in time integration, *Int. J. Num. Meth. Eng.* **12**, 1575–1586 (1978)
33 Belytschko, T., Yen, H. J. and Mullen, R. Mixed methods for time integration, *Comp. Meth. Appl. Mech. Eng.*, **17/18**, 259–275 (1979)
34 Irons, B. M. Application of a theorem on eigen values to finite element problems, *Res. Rep. C/R/132/70*, Civil Eng. Dept., Univ. of Wales, Swansea (1970)
35 Hinton, E., Rock, T. and Zienkiewicz, O. C. A note on mass lumping and related processes in the finite element method, *Earthq. Eng. Struct. Dyn.*, **4**, 245–249 (1976)
36 Surana, K. S. Lumped mass matrices with non-zero inertia for general shell and axi-symmetric shell elements, *Int. J. Num. Meth. Eng.*, **12**, 1635–1650 (1978)
37 Geers, T. L. Excitation of an elastic shell by a transient acoustic wave, *ASME J. Appl. Mech.*, **36**, 459–469 (1969)
38 Geers, T. L., Boundary element methods for transient response analysis, *Computational Methods for Transient Analysis* (Eds. Belytschko, T. and Hughes, T. J. R.) Elsevier, Amsterdam, Ch. 4 (1983)